NANO · MICRO small
www.small-journal.com

A New Support Film for Cryo Electron Microscopy Protein Structure Analysis Based on Covalently Functionalized Graphene

Philip Nickl, Tarek Hilal, Daniel Olal, Ievgen Sergeevitch Donskyi, Jörg Radnik, Kai Ludwig,* and Rainer Haag**

Dedicated to the 70th birthday of Professor Matthias Ballauff

Protein adsorption at the air–water interface is a serious problem in cryogenic electron microscopy (cryoEM) as it restricts particle orientations in the vitrified ice-film and promotes protein denaturation. To address this issue, the preparation of a graphene-based modified support film for coverage of conventional holey carbon transmission electron microscopy (TEM) grids is presented. The chemical modification of graphene sheets enables the universal covalent anchoring of unmodified proteins via inherent surface-exposed lysine or cysteine residues in a one-step reaction. Langmuir–Blodgett (LB) trough approach is applied for deposition of functionalized graphene sheets onto commercially available holey carbon TEM grids. The application of the modified TEM grids in single particle analysis (SPA) shows high protein binding to the surface of the graphene-based support film. Suitability for high resolution structure determination is confirmed by SPA of apoferritin. Prevention of protein denaturation at the air–water interface and improvement of particle orientations is shown using human 20S proteasome, demonstrating the potential of the support film for structural biology.

1. Introduction

Single particle cryoEM emerged as a powerful tool for reconstructing protein structures in structural biology, and even more so after significant technical breakthroughs.[1,2] The development of direct electron detectors and improvements in data analysis nowadays allow for reconstruction of protein structures with near-atomic and in certain cases even with atomic resolution.[3] While the technical setup of electron microscopes has been steadily refined over decades, development of cryogenic sample preparation lagged behind.[4,5,6,7] Usually, metal grids covered with an amorphous holey carbon film are used for preparation of vitrified biological samples. In general, the protein solution is applied to the grid and excess solution is removed by mechanical blotting before the grid is plunged into liquid ethane, which ideally traps the particles in random orientation and with even distribution inside the vitreous ice-film.[8] However, proteins have been shown to often adsorb at the air–water interface which provokes preferential orientation, uneven particle distribution inside the ice-film or structural changes of the proteins, at worst resulting in protein denaturation.[9,10] In single particle cryoEM, the 3D reconstruction of an object relies on backprojection of numerous 2D projections of the same particle in different orientations.[11] Consequently, a successful 3D reconstruction strongly depends on the prevention of preferred particle orientation during vitrification.[12] To this end, various support film-based strategies for non-covalent protein adsorption have been developed in the past, including nanobodies,[13] DNA scaffolds,[14] lipid monolayers,[15] or streptavidin crystals.[16] Since such approaches lower the overall contrast of biological samples due to the introduction of additional biomass, graphene-based monolayer support films have emerged as favored sample support in single particle cryoEM as they are intrinsically transparent, excellent electrically conductive and possess high mechanical strength.[17,18,19,20,21] Although graphene-based support films have proven as valuable approach to overcome adsorption of particles at the air–water interface, binding of the sample is uncontrolled.[22] Consequently, graphene-based

P. Nickl, I. S. Donskyi, R. Haag
Institut für Chemie und Biochemie
Freie Universität Berlin
Takustr. 3, 14195 Berlin, Germany
E-mail: haag@chemie.fu-berlin.de
P. Nickl, T. Hilal, D. Olal, K. Ludwig
Forschungszentrum für Elektronenmikroskopie und Core Facility BioSupraMol
Institut für Chemie und Biochemie
Freie Universität Berlin
Fabeckstr. 36a, 14195 Berlin, Germany
E-mail: tarek.hilal@fzem.fu-berlin.de; kai.ludwig@fzem.fu-berlin.de
P. Nickl, I. S. Donskyi, J. Radnik
Division 6.1 – Surface Analysis and Interfacial Chemistry
BAM – Federal Institute for Material Science and Testing
Unter den Eichen 44-46, 12205 Berlin, Germany

The ORCID identification number(s) for the author(s) of this article can be found under https://doi.org/10.1002/smll.202205932.

DOI: 10.1002/smll.202205932

support films have been further modified with so-called affinity tags, that enable the selective non-covalent anchoring of biomolecules on the grid.[23] Nitrilotriacetic acid functionalized graphene films loaded with Ni^{2+} ions have been successfully reported for selective targeting and anchoring of Histidine-tagged (His) proteins.[24,25] However, this approach is limited to His-tagged proteins only and since the tag is usually introduced at one of the ends of the polypeptide chain, preferential protein orientation cannot be excluded. Recently, more sophisticated strategies for covalent anchoring of proteins have been reported, including Spy-catcher tags.[26]

Here, we present a simple sample support film for cryoEM, based on thermally reduced graphene oxide (TRGO) sheets that are covalently functionalized with dichloro-triazine moieties (TRGO-Trz). The functional moieties enable the covalent conjugation of target proteins in a non-specific way via nucleophilic aromatic substitution of one of the chlorine atoms by surface exposed lysine or cysteine residues. In the first step, high quality TRGO sheets with a uniform size distribution, obtained through bulk synthesis, reported by Müllhaupt et al.,[27] were covalently functionalized by nitrene-[2+1]-cycloaddition using 2-azido-4,6-dichloro-1,3,5-triazine yielding dichloro-triazine-functionalized sheets. After functionalization, the graphene sheets are deposited in a controlled way onto commercially available holey carbon TEM grids using LB trough technique,[28] resulting in sample support film covered holey carbon TEM grids for high-resolution cryoEM (**Scheme 1**). We carefully characterized the TRGO-Trz-based support film modified TEM grids and demonstrated its potential application for SPA using apoferritin and human 20S proteasome as model proteins.

2. Results and Discussion

Pristine TRGO sheets were functionalized according to the previously established nitrene [2+1]-cycloaddition protocol.[29,30] Briefly, TRGO-Trz sheets were obtained in an one-pot-reaction. Here, TRGO sheets dispersed in *N*-Methyl-2-pyrrolidone (NMP) reacted with 2-azido,4,6-dichloro-1,3,5-triazine, which was prepared by reaction between sodium azide (NaN_3) and 2,4,6-trichloro-1,3,5-triazine (TCT) in NMP at 0 °C. All synthesis steps were monitored by x-ray photoelectron spectroscopy (XPS) and near-edge x-ray adsorption fine structure spectroscopy (NEXAFS). To verify the protein binding capability of the functionalized graphene sheets, HEPES-buffered apoferritin solution (Sigma A3660) was mixed with TRGO-Trz sheets and incubated for 3 min at 30 °C and carefully washed afterward. For pristine TRGO, XP survey spectrum only contains peaks at 530 and 285 eV, which can be assigned to O1s and C1s, respectively (**Figure 1**G). Moreover, the survey spectrum for TRGO-Trz contains an additional peak at 400 eV, referring to nitrogen N1s arising from the successful introduction of dichloro-triazine moieties to TRGO. After protein conjugation, the survey spectrum of TRGO-Trz-apoferritin contains three main peaks at 530 eV (O1s), 400 eV (N1s), and 285 eV (C1s). From the highly resolved carbon 1s XP spectrum, the dominant chemical component for TRGO at 284.8 eV could be assigned

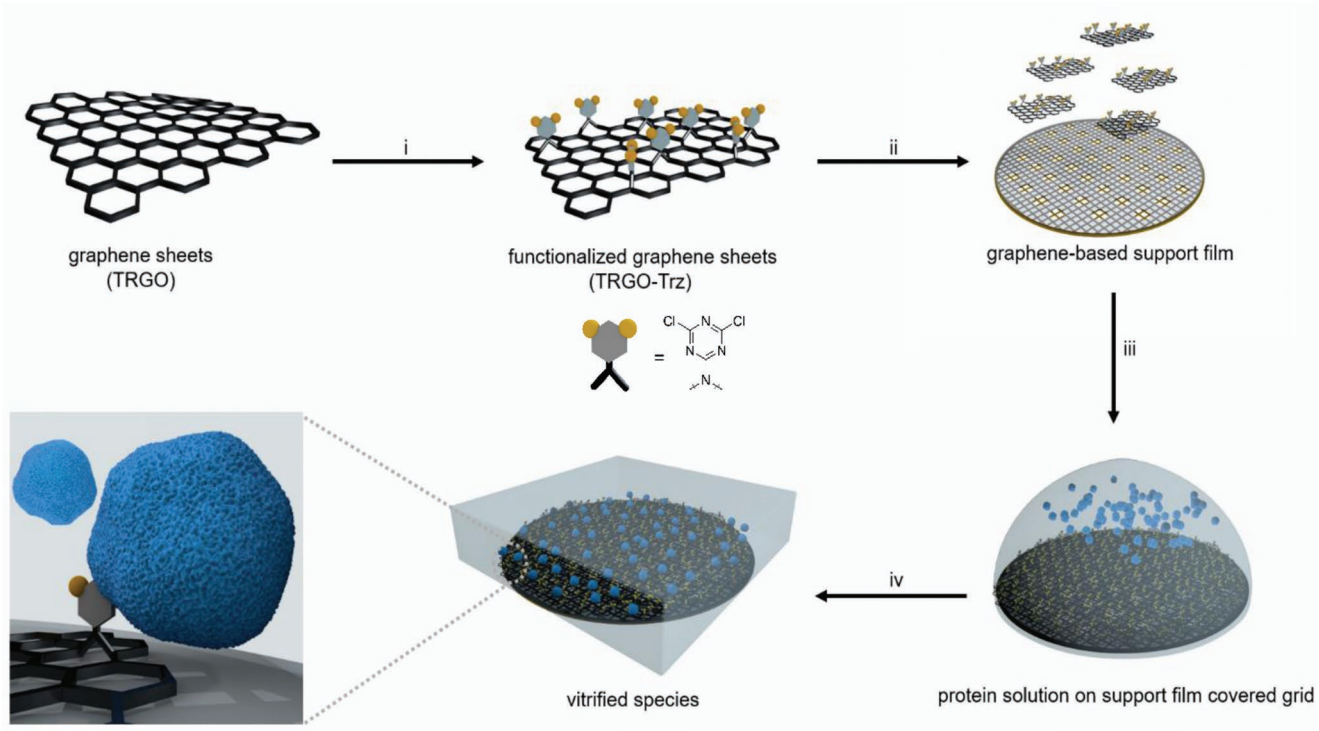

Scheme 1. Schematic representation of sample support film preparation: graphene sheets are functionalized by nitrene [2+1]-cycloaddition and deposited onto standard holey carbon TEM grids by LB trough. Support film covered TEM grids are applied in cryoEM showing high protein binding. i) NaN_3, TCT, NMP, 70 °C, 12 h; ii) LB trough, MeOH: H_2O 1:11; iii) buffered protein solution, 30 °C, 3 min; iv) blotting and vitrification.

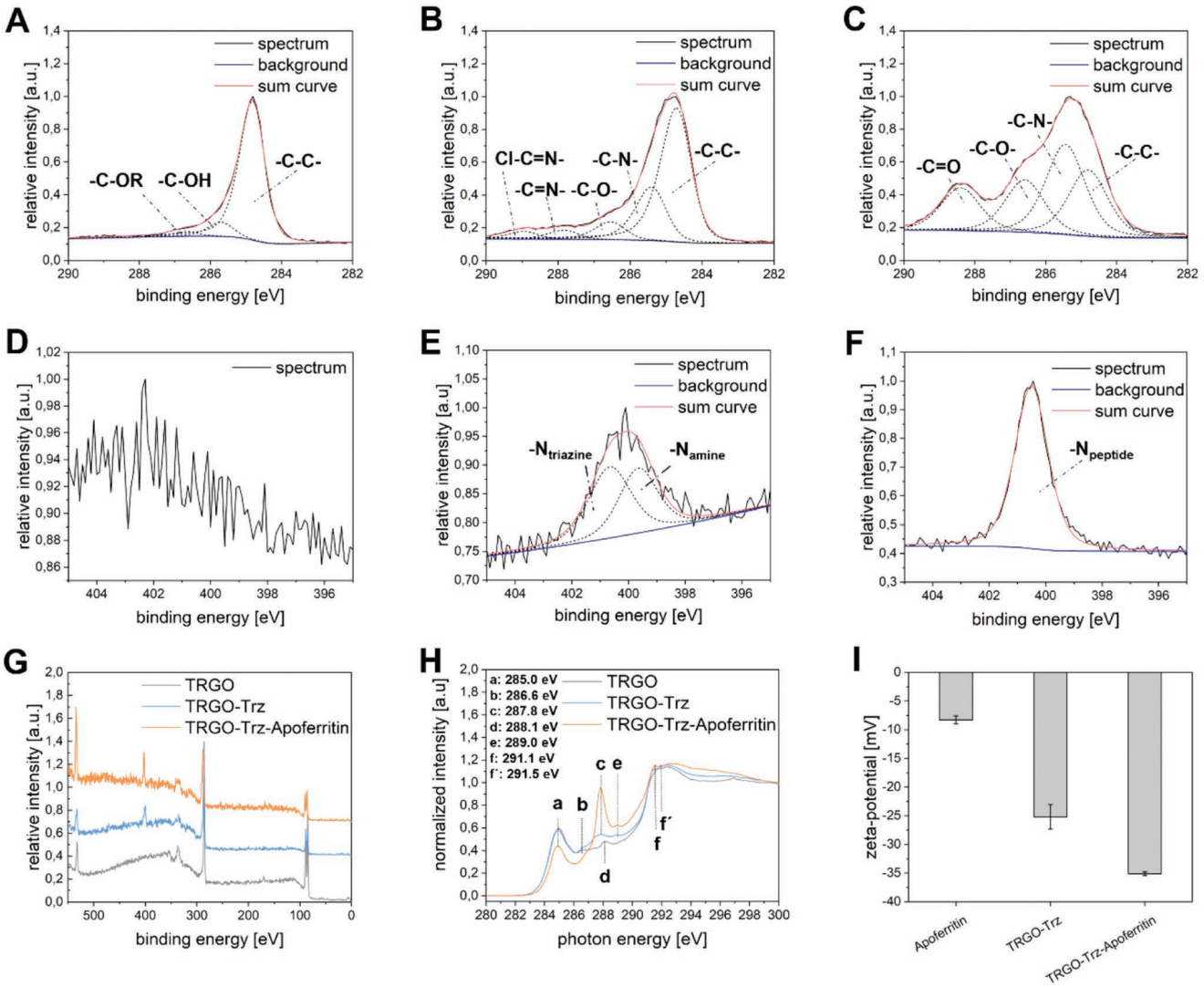

Figure 1. Characterization of functionalized graphene sheets before and after protein binding. Highly resolved C1s XP spectra for A) TRGO, B) TRGO-Trz, and C) TRGO-Trz-apoferritin. Highly resolved N1s XP spectra for D) TRGO, E) TRGO-Trz, and F) TRGO-Trz-apoferritin. G) XP survey spectra for TRGO, TRGO-Trz, and TRGO-Trz-apoferritin. H) Normalized C K near-edge x-ray absorption fine structure spectra for pristine TRGO, TRGO-Trz, and TRGO-Trz-apoferritin. I) Zeta-potential for apoferritin, TRGO-Trz and TRGO-Trz-apoferritin in HEPES buffer medium at pH = 7.6.

to sp^2-hybridized carbon species and only a low number of oxygen-containing defects contributed to small peaks at higher binding energies between 285 and 287 eV (Figure 1A).

After conjugation of apoferritin, the major chemical components for TRGO-Trz-apoferritin were found in a binding energy regime between 286 and 289 eV (Figure 1C). The chemical component at 285.6 eV could be assigned to C—N— and C—O-containing chemical species, while peaks at 287.1 and at 288.8 eV could be assigned to C=O— and N—C=O-containing chemical species, respectively. Especially the peaks at 287.1 eV (—C=O) and 288.8 eV (—N—C=O) are typical for chemical species comprised of peptides and proteins, indicating the successful conjugation of apoferritin to TRGO-Trz. For the highly resolved N1s XP spectrum of TRGO, no signal is found (Figure 1D), while highly resolved N1s spectrum of TRGO-Trz is composed of two peaks at 399.6 and 400.7 eV, referring to aziridine nitrogen and aromatic nitrogen chemical states of the triazine core, respectively[30] (Figure 1E). For TRGO-Trz-apoferritin, the main component of the highly resolved N1s spectrum was found at 400.5 eV corresponding to nitrogen atoms in the peptide bonds (Figure 1F and Table S1, Supporting Information). The C K-edge NEXAFS spectrum for pristine TRGO was composed of various transitions from C 1s orbitals to empty, bound final states (Figure 1H). At the lower energy side, a sharp resonance at a photon energy of 284.8 eV corresponds to C1s π^* transition of sp^2-hybridized carbon species. At higher binding energy side, a second sharp resonance arouse at 292 eV referring to C1s σ^* transition of sp^3-hybridized carbon species. For TRGO-Trz, all TRGO-corresponding resonance features were observable in the carbon K-edge NEXAFS spectrum, but also new resonances corresponding to the dichloro-triazine moieties occurred in the photon energy regime between 285 and 290 eV.[29] After functionalization, the resonance intensity ratio of C1s π^* transition to C1s σ^* transitions did not change,

indicating the successful preservation of the aromatic π-system. After conjugation of apoferritin to TRGO-Trz, all TRGO-Trz-corresponding resonance features could be observed. Additionally, a second very strong resonance at 288.1 eV was apparent, which could be assigned to C1s π^* transition of C=O-containing peptide bonds of the protein, confirming the conjugation of apoferritin to the TRGO-Trz. Furthermore, the resonance intensity ratio of C1s π^* transition to C1s σ^* transitions decreased significantly due to the relative high number of sp^3-hybridized carbon species of the protein.

The ζ-potential for pristine TRGO-Trz in buffer medium (pH = 7.6) was found to be −25 mV and to be −8.0 mV for apoferritin, indicating that non-specific interaction between the support film and protein is unfavored with respect to the surface charge. After conjugation, the ζ-potential of TRGO-Trz-apoferritin changed to −35 mV (Figure 1I).

As a next step, the sample support film for cryoEM was prepared by deposition of functionalized graphene onto standard holey carbon TEM grids using a LB trough (Figure S1, Supporting Information). Here, conventional holey carbon TEM grids were placed at the bottom of the trough filled with water-methanol solution (11:1). After a dispersion of TRGO-Trz sheets in a water–methanol solution (1:1) was carefully dropped onto the solution's surface, the sheets were deposited onto the grids by a slow drain of solution from the trough. Successful deposition of functionalized graphene sheets could be confirmed by typical Bragg reflections from electron irradiation (Figure S6, Supporting Information). To investigate if our support film and the chemical coupling reaction interferes with structural analysis by cryoEM, we chose apoferritin as a test specimen. Apoferritin is a well-established model protein in electron microscopy due to its outstanding robustness and high degree of symmetry, which allows reconstructions with near-atomic resolution.[31] We performed the coupling reaction of apoferritin to the TRGO-Trz covered grids for 3 min at 30 °C under controlled ambient conditions in the Vitrobot chamber to ensure proper protein binding. Excess solution was removed by conventional blotting before vitrification in liquid ethane.

The correspondingly prepared cryogrids revealed a uniform distribution of apoferritin particles with high density coupled to the support film (**Figure 2**A). To confirm that particles were chemically coupled rather than physically adsorbed, we performed control experiments by washing the film with buffer (Figure S2, Supporting Information) after the reaction. Apoferritin particles were still present in high quantity after washing, supporting that binding was mediated by coupling through the dichloro-triazine moieties. Ultimately, to confirm that our coupling approach preserved protein structure, single particles analysis was conducted. The obtained 3D reconstruction (Figure 2C) had a global resolution of 2.95 Å, locally extending up to 2.6 Å with individual protein side chains clearly resolved (Figure S3, Supporting Information). Most notably, the reconstruction is virtually indistinguishable from a control sample prepared on standard holey carbon grids (Figure 2B), indicating that our support film as well as the coupling reaction preserve protein integrity (Figure S4, Supporting Information) for the tested specimen.

We then asked whether our support film has beneficial effects on samples with unfavorable behavior. The human 20S proteasome is a common test specimen used in cryoEM as it has easy to distinguish top and side views. However, due to adsorption at the air–water interface,[32] human 20S proteasome is prone to aggregation during vitrification without support film. When applied to non-functionalized support film covered TEM grids, most of the protein particles are trapped in the top-view orientation preventing successful 3D reconstruction.[33]

We compared cryo preparations of human 20S proteasome on standard holey carbon TEM grids (Figure S5, Supporting Information) with preparations on our TRGO-Trz support (Figure S4, Supporting Information). Strikingly, only samples applied to the TRGO-Trz support film show intact particles giving rise to further evaluation by 2D classification (**Figure 3**A). Evaluation of the obtained class averages (Figure S7, Supporting Information) reveals pre-dominance of top views (82%) over side views (18%). To further investigate, if covalently conjugated particles behave different from non-covalently adsorbed particles, additional grids were prepared including a washing step. To this end, after the coupling reaction was completed, excess liquid was removed and replaced with sample buffer on the grid twice before vitrification (Figure 3B). Despite an obvious reduction in total particle concentration on the grid, analysis

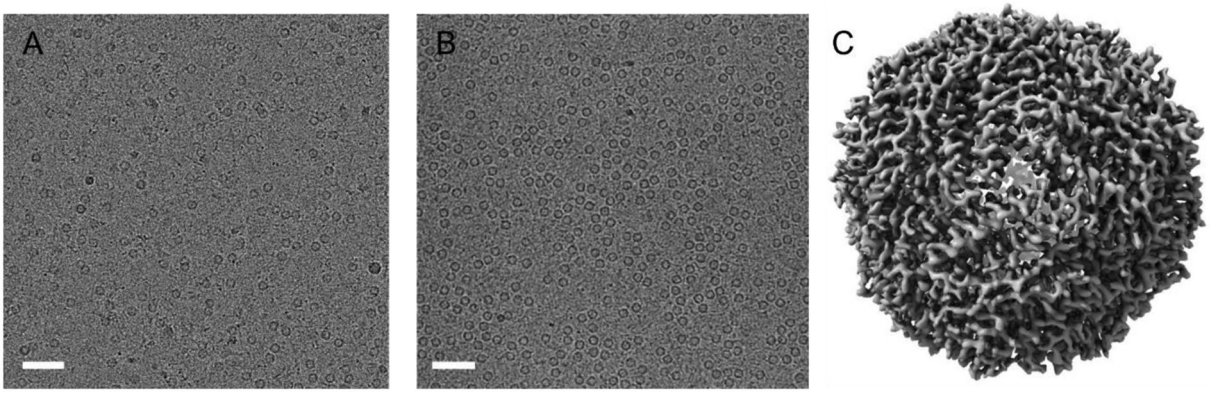

Figure 2. Application of the sample support film in single particle cryoEM analysis: A) representative micrograph illustrating apoferritin on graphene film and B) on standard holey carbon TEM grids without support film. C) 3D reconstruction of apoferritin on top of sample support film. Scale bars correspond to 50 nm.

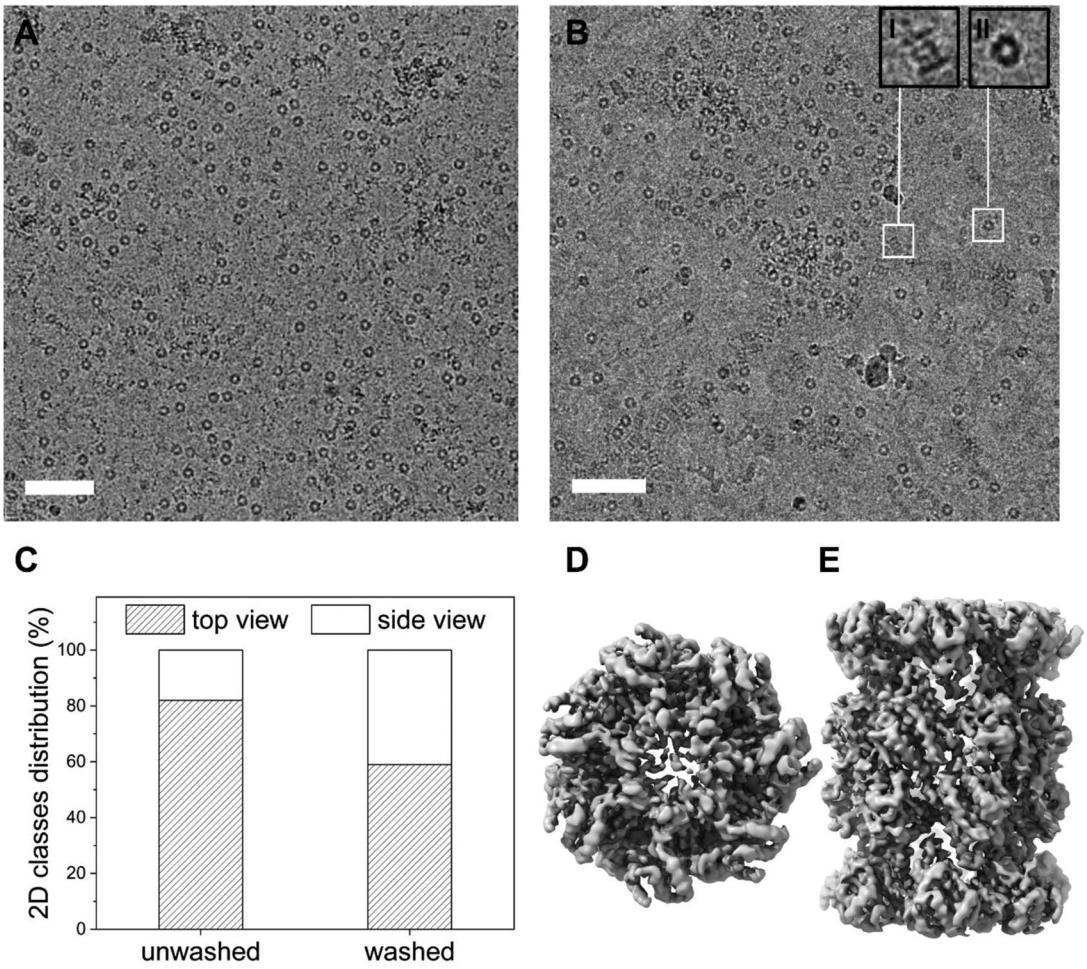

Figure 3. Micrographs of vitrified human 20S proteasome on A) support-film covered TEM grids and B) support-film covered TEM grids including one washing step between sample application and vitrification—insets showing 20S proteasome with I) side view orientation and II) top view orientation. C) 2D class distribution for 20S proteasome on support-film covered grids with and without washing after sample application. 3D cryoEM map of human 20S proteasome in D) top view and E) side view orientation. Scale bars correspond to 50 nm.

by 2D classification revealed a significant change in the distribution of particle orientations (Figure S8, Supporting Information). After washing, we find 59% top-view and 41% side-view projections as determined by 2D classification, demonstrating efficient randomization of 20S proteasome orientations (Figure 3C). Capitalizing the improved distribution of top and side-views, a 3D reconstruction of the human 20S proteasome at 2.7 Å resolution could be generated (Figure 3D,E). To further visualize the distribution of protein particles within the ice layer, cryo electron tomography (cryo-ET) was employed (**Figure 4**), revealing proteasome particles in high density exclusively attached to the support film (Figure 4A–C). Notably, the nearly equal distribution of side-view and top-view orientations obtained by SPA are confirmed by cryo-ET (Figure 4D).

Prospectively, our presented graphene-based support film can be used as versatile tool for coupling of various moieties. The temperature dependent substitution of the two chlorine atoms attached to the triazine moieties[29] allows the controlled and stepwise post-modification with, e.g., chemical linkers for protein binding at low temperatures, structurally flexible or hydrophilic linker molecules, enabling the tailoring of more customized support film materials for analysis of more fragile protein species. Besides the chemical linkage of proteins by amine-coupling, also DNA- or RNA-fragments can be conjugated to the triazine moieties. This allows for direct interaction studies of nucleic acid binding proteins on the grid or permits affinity-based purification from heterogeneous samples.[26]

3. Conclusion

In summary, we present a simple sample support material for structural cryoEM analysis of biomacromolecules based on functionalized graphene sheets. The protein of interest can be covalently anchored to the developed support film through intrinsic lysine or cysteine residues. Capability for high resolution structure determination was confirmed by single particle analysis of apoferritin. Prevention of protein denaturation at the air–water interface and improvement of particle orientation distribution after covalent coupling could be demonstrated by studies of human 20S proteasome. We envision the application of our developed sample support as platform for

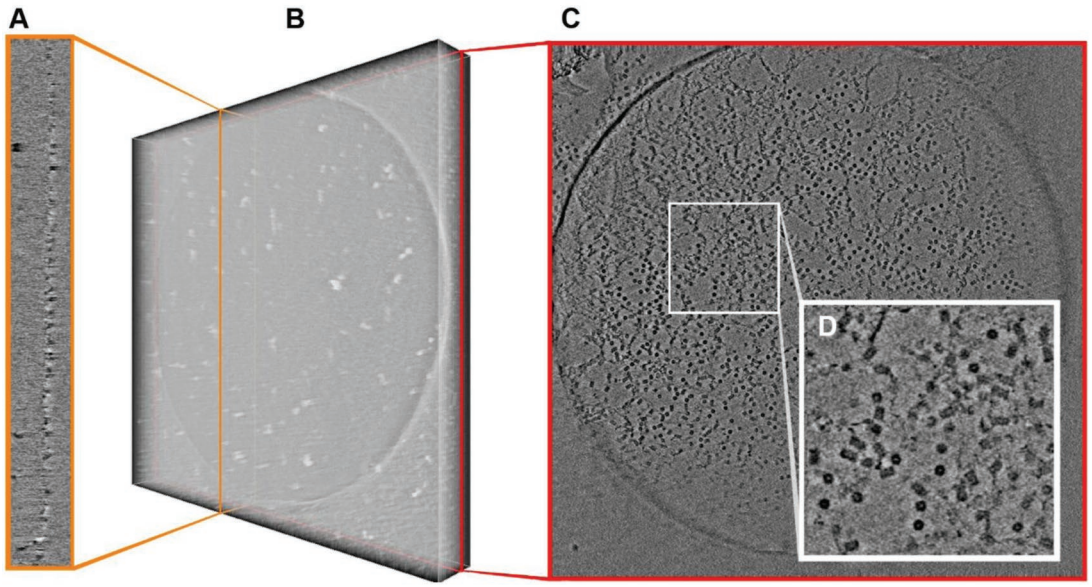

Figure 4. Cryo-electron tomogram of human 20S proteasome coupled to support film after washing. A) *yz*-slice from the reconstructed 3D volume, the position is marked with an orange frame in (B). Single large cryo-contaminations are localized on the surface of the amorphous ice film, protein particles are exclusively coupled to the support film. B) "Voltex" visualization of the reconstructed 3D volume rotated 45° around the *y*-axis (note the contrast inversion) C) *xy*-slice from the 3D volume on the level of the support film (marked with a red frame in (B)) showing the uniform distribution of protein particles on the support film. D) Enlarged section marked by a white frame in (C) showing individual top- and side-view particles.

target-protein-driven tailoring of individual sample support films according to the experimental requirements.

Supporting Information

Supporting Information is available from the Wiley Online Library or from the author.

Acknowledgements

The core facility BioSupraMol is acknowledged for technical support and Benedikt Kirmayer for cryoEM sample preparation. The authors are also grateful to PD. Dr. Christoph Böttcher for fruitful discussions, Dr. Siegfried Eigler for providing the LB trough and Dr. Regina Eigler for introduction to the LB trough. The authors further would like to acknowledge the Helmholtz Zentrum Berlin (HZB) team at the HE-SGM beamline located at the BESSY II synchrotron radiation facility as well as Dr. A. Nefedov (Karlsruher Institute of Technology, KIT) and Dr. M. Brzhezinskaya (HZB Berlin) from the HE-SGM collaborate research group. M.Sc. Taylor Page is acknowledged for careful proofreading of the manuscript.

Open access funding enabled and organized by Projekt DEAL.

Conflict of Interest

The authors declare no conflict of interest.

Data Availability Statement

The data that support the findings of this study are available in the Supporting Information of this article.

Keywords

cryogenic electron microscopy, cryogenic electron tomography, graphene, single particle analysis, support films, x-ray photoelectron spectroscopy

Received: September 27, 2022
Revised: November 25, 2022
Published online:

[1] X.-c. Bai, G. McMullan, S. H. W. Scheres, *Trends Biochem. Sci.* **2015**, *40*, 49.
[2] Y. Cheng, *Science* **2018**, *361*, 876.
[3] R. Strack, *Nat. Methods* **2020**, *17*, 1175.
[4] K. Murata, M. Wolf, *Biochim. Biophys. Acta, Gen. Subj.* **2018**, *1862*, 324.
[5] K. R. Vinothkumar, R. Henderson, *Q. Rev. Biophys.* **2016**, *49*, e13.
[6] M. Adrian, J. Dubochet, J. Lepault, A. W. McDowall, *Nature* **1984**, *308*, 32.
[7] R. A. Grassucci, D. J. Taylor, J. Frank, *Nat. Protoc.* **2007**, *2*, 3239.
[8] A. Doerr, *Nat. Methods* **2016**, *13*, 23.
[9] R. M. Glaeser, *Curr. Opin. Colloid Interface Sci.* **2018**, *34*, 1.
[10] A. J. Noble, H. Wei, V. P. Dandey, Z. Zhang, Y. Z. Tan, C. S. Potter, B. Carragher, *Nat. Methods* **2018**, *15*, 793.
[11] D. J. De Rosier, A. Klug, *Nature* **1968**, *217*, 130.
[12] A. J. Noble, V. P. Dandey, H. Wei, J. Brasch, J. Chase, P. Acharya, Y. Z. Tan, Z. Zhang, L. Y. Kim, G. Scapin, M. Rapp, E. T. Eng, W. J. Rice, A. Cheng, C. J. Negro, L. Shapiro, P. D. Kwong, D. Jeruzalmi, A. des Georges, C. S. Potter, B. Carragher, *eLife* **2018**, *7*, e34257.
[13] T. Uchański, S. Masiulis, B. Fischer, V. Kalichuk, U. López-Sánchez, E. Zarkadas, M. Weckener, A. Sente, P. Ward, A. Wohlkönig, T. Zögg, H. Remaut, J. H. Naismith, H. Nury, W. Vranken, A. R. Aricescu, E. Pardon, J. Steyaert, *Nat. Methods* **2021**, *18*, 60.

[14] D. N. Selmi, R. J. Adamson, H. Attrill, A. D. Goddard, R. J. C. Gilbert, A. Watts, A. J. Turberfield, *Nano Lett.* **2011**, *11*, 657.
[15] D. F. Kelly, D. Dukovski, T. Walz, *J. Mol. Biol.* **2010**, *400*, 675.
[16] B.-G. Han, Z. Watson, J. H. D. Cate, R. M. Glaeser, *J. Struct. Biol.* **2017**, *200*, 307.
[17] A. A. Balandin, S. Ghosh, W. Bao, I. Calizo, D. Teweldebrhan, F. Miao, C. N. Lau, *Nano Lett.* **2008**, *8*, 902.
[18] Y. Wang, Y. Chen, S. D. Lacey, L. Xu, H. Xie, T. Li, V. A. Danner, L. Hu, *Mater. Today* **2018**, *21*, 186.
[19] R. S. Pantelic, J. C. Meyer, U. Kaiser, H. Stahlberg, *Solid State Commun.* **2012**, *152*, 1375.
[20] C. Lee, X. Wei, J. W. Kysar, J. Hone, *Science* **2008**, *321*, 385.
[21] A. K. Geim, K. S. Novoselov, *Nat. Mater.* **2007**, *6*, 183.
[22] C. J. Russo, L. A. Passmore, *Nat. Methods* **2014**, *11*, 649.
[23] M. R. Hoq, F. S. Vago, K. Li, M. Kovaliov, R. J. Nicholas, D. M. Huryn, P. Wipf, W. Jiang, D. H. Thompson, *ACS Nano* **2021**, *15*, 8376.
[24] C. J. Benjamin, K. J. Wright, S. C. Bolton, S.-H. Hyun, K. Krynski, M. Grover, G. Yu, F. Guo, T. L. Kinzer-Ursem, W. Jiang, D. H. Thompson, *Sci. Rep.* **2016**, *6*, 32500.
[25] N. Liu, J. Zhang, Y. Chen, C. Liu, X. Zhang, K. Xu, J. Wen, Z. Luo, S. Chen, P. Gao, K. Jia, Z. Liu, H. Peng, H.-W. Wang, *J. Am. Chem. Soc.* **2019**, *141*, 4016.
[26] F. Wang, Y. Liu, Z. Yu, S. Li, S. Feng, Y. Cheng, D. A. Agard, *Proc. Natl. Acad. Sci. U. S. A.* **2020**, *117*, 24269.
[27] B. Schlüter, R. Mülhaupt, A. Kailer, *Tribol. Lett.* **2014**, *53*, 353.
[28] L. J. Cote, F. Kim, J. Huang, *J. Am. Chem. Soc.* **2009**, *131*, 1043.
[29] A. Faghani, I. S. Donskyi, M. Fardin Gholami, B. Ziem, A. Lippitz, W. E. S. Unger, C. Böttcher, J. P. Rabe, R. Haag, M. Adeli, *Angew. Chem.* **2017**, *129*, 2719.
[30] G. Guday, I. S. Donskyi, M. F. Gholami, G. Algara-Siller, F. Witte, A. Lippitz, W. E. S. Unger, B. Paulus, J. P. Rabe, M. Adeli, R. Haag, *Small* **2019**, *0*, 1805430.
[31] T. Nakane, A. Kotecha, A. Sente, G. McMullan, S. Masiulis, P. M. G. E. Brown, I. T. Grigoras, L. Malinauskaite, T. Malinauskas, J. Miehling, T. Uchański, L. Yu, D. Karia, E. V. Pechnikova, E. de Jong, J. Keizer, M. Bischoff, J. McCormack, P. Tiemeijer, S. W. Hardwick, D. Y. Chirgadze, G. Murshudov, A. R. Aricescu, S. H. W. Scheres, *Nature* **2020**, *587*, 152.
[32] R. M. Glaeser, *Annu. Rev. Biochem.* **2021**, *90*, 451.
[33] P. C. A. da Fonseca, E. P. Morris, *Nat. Commun.* **2015**, *6*, 7573.